Choosing meteorological input for the global modeling initiative assessment of high speed aircraft

A. R. Douglass,[1] M. P. Prather,[2] T. M. Hall,[3] S. E. Strahan,[4] P. J. Rasch, [5] L. C. Sparling, [6] L. Coy [4] and J. M. Rodriguez [7]

Short title:

Abstract. The Global Modeling Initiative (GMI) science team is developing a three dimensional chemistry and transport model (CTM) to be used in assessment of the atmospheric effects of aviation. Requirements are that this model be documented, be validated against observations, use a realistic atmospheric circulation, and contain numerical transport and photochemical modules representing atmospheric processes. The model must also retain computational efficiency to be tractable to use for multiple scenarios and sensitivity studies. To meet these requirements, a facility model concept was developed in which the different components of the CTM are evaluated separately. The first use of the GMI model will be to evaluate the impact of the exhaust of supersonic aircraft on the stratosphere. The assessment calculations will depend strongly on the wind and temperature fields used by the CTM. Three meteorological data sets for the stratosphere are available to GMI: the National Center for Atmospheric Research Community Climate Model (CCM2), the Goddard Earth Observing System Data Assimilation System (GEOS DAS), and the Goddard Institute for Space Studies general circulation model (GISS).

Objective criteria were established by the GMI team to identify the data set which provides the best representation of the stratosphere. Simulations of gases with simple chemical control were chosen to test various aspects of model transport. The three meteorological data sets were evaluated and graded based on their ability to simulate these aspects of stratospheric measurements. This paper describes the criteria used in grading the meteorological fields. The meteorological data set which has the highest score and therefore was selected for GMI is CCM2. This type of objective model evaluation establishes a physical basis for interpretation of differences between models and observations. Further, the method provides a quantitative basis for defining model errors, for discriminating between different models, and for ready re-evaluation of improved models. These in turn will lead to a higher level of confidence in assessment calculations.

1. Introduction

The Atmospheric Effects of Stratospheric Aircraft (AESA) component of the National Aeronautics and Space Administration (NASA) High Speed Research Program (HSRP) seeks to assess the impact of a fleet of high speed civil transport (HSCT) aircraft on the lower stratosphere. There are several components to such an assessment. Measurements in the field and laboratory, characterization of the exhaust products, and development of realistic scenarios for the distribution of emissions all play important roles. Ultimately, the use of models to calculate the fate of aircraft exhaust, the buildup of such pollution in the lower stratosphere, and the model response of ozone to the change in lower stratospheric composition is a key element of the assessment, as models are the primary tools through which the impact on the ozone layer is quantified.

Assessment calculations for stratospheric aircraft have centered on results obtained with two dimensional (latitude altitude) models [*Prather et al.,* 1992; *Stolarski et al.,* 1995]. However, as has been pointed out from the start of AESA [*Douglass et al.,* 1991], there are aspects to this assessment which are more appropriately modeled in three dimensions. The aircraft are proposed to fly mainly in the northern hemisphere and always over the oceans with a high concentration of flight paths in identifiable oceanic corridors. Thus the pollutant source is zonally asymmetric and concentrated. The meteorology of the northern hemisphere stratosphere is influenced by the land ocean pattern, thus the transport of polluted air from the stratosphere to the troposphere is also asymmetric. There have been efforts to evaluate the importance of these asymmetries to the assessment calculation, and to quantify expected differences from a two dimensional calculation [*Douglass et al.,* 1993; *Rasch et al.,* 1994; *Weaver et al.,* 1995; *Weaver et al.,* 1996]. Although studies so far suggest fairly small impacts to the build up of exhaust for three dimensional (3D) versus two dimensional (2D) models, uncertainties remained. There were differences in the pollutant build-up and the ozone response calculated by the various 2D models, which focussed attention on

uncertainty in the 2D model transport. The National Research Council Panel on the AESA reviewed the NASA Interim Assessment [*Albritton et al.*, 1993], recognized this uncertainty, and recommended greater use of three-dimensional models, at least to evaluate the uncertainties associated with transport [*Graedel et al.*, 1994].

There are fundamental advantages to a three dimensional calculation using state of the art representations of stratospheric chemical and transport processes, all of which could serve to reduce uncertainty in the assessment calculation, a primary goal of the AESA. Some of the uncertainties in the 2D model assessments arise because there are observed aspects of stratospheric transport that are not represented explicitly in 2D models. These include (but are not limited to) the wave mean flow interaction, the seasonal variation in the tropopause height, cross tropopause transport, and the seasonal evolution of the polar vortices. The 2D models adopt diffusion coefficients to simulate the 3D mixing of trace gases by planetary scale waves and to define the tropopause. While there is a strong theoretical basis for collapsing stratospheric transport to two dimensions, formulation of a 2D model requires simplifying assumptions, and the formulations in current use are not unique, as evidenced by the range of results for model transport tests as reported by the Second Stratospheric Models and Measurements Workshop [*Ko and Jackman*, 1999].

The 3D models address these uncertainties by improving the physical basis for representing these processes. In some cases, comparisons of models with observations reflect these improvements. For example, the amplitude of the annual cycle in total ozone at northern middle latitudes is generally closer to the observed amplitude in 3D models than in 2D models [*Rasch et al.*, 1995; *Douglass et al.*, 1996]. The improved agreement is at least partially a result of a more physical representation of the tropopause and the concomitant transport in the lowermost stratosphere. It is important to remember that 2D models have long been used to calculate constituent evolution, and comparison of calculated fields with zonal means of global observations

has been a principle means of evaluating the 2D models [e.g., *Prather and Remsberg,* 1993]. As noted above, model transport has a strong theoretical basis, but retains a strong phenomenological component due to underlying simplifying assumptions and parameterizations. The 3D models do not have this heritage for constituent modeling, and it is not likely that they will produce zonal mean results that compare better with zonal mean observations than 2D models. However, improvement in the physical basis of the models sets the stage for physically based improvements in the 3D model, often through interpretation of the differences between model fields and constituent observations.

The major disadvantage to utilizing 3D models for assessment is their large computational requirement. Since the motivation for using the 3D model rests on the improved physical basis of the model, the horizontal and vertical resolution must be adequate to resolve important transport processes. The transport and photochemical time steps must both be substantially smaller than the time steps often used in 2D models. Model evaluation also becomes a larger task, requiring both computational and human resources. It is impractical that 3D assessments follow the path of 2D assessments, in which independent calculations are produced by several research groups. To gain the benefits of using the 3D assessment and maintain involvement of several research groups, the Global Modeling Initiative (GMI) science team was formed.

The goal of this group is to produce a well tested 3D chemistry and transport model that is useful for assessment calculations. A modular design allows various numerical transport schemes, photochemical schemes, and sets of meteorological data (winds and temperatures) to be tested within a common framework. The choices of which scheme to use have been made considering both performance and computational requirements. The choices for the numerical scheme for photochemistry [*Connell et al.,* 1998] and transport [*Rotman et al.,* 1998], and the initial results from an assessment calculation [*Kinnison et al.,* 1998] are presented in companion papers in this issue. This

paper centers on establishing criteria to choose the meteorological input fields for the assessment model.

This exercise of evaluating different meteorological fields for use in the model sets an important precedent for modeling work. The models are evaluated strictly by comparisons with observations, and are scored quantitatively relative to each other and to a standard defined by the observations. The approach given here provides a quantitative, reproducible method for evaluating a meteorological data set. Because the tests are themselves physically based, this provides groundwork for identification of needed model improvements. Application of the same tests to improved models will give a quantitative measure of the improvements. In the future the tests may be applied to other meteorological data sets; the tests themselves may be refined, expanded, replaced, or augmented. However, the methodology should stand, and serves as a challenge to move from subjective to quantitative model evaluation. An obvious extension to this application will be evaluation of the tropospheric and lower stratospheric transport produced by various meteorological data sets as part of the Atmospheric Effects of Aircraft Project (AEAP) Subsonic Assessment (SASS), also an objective of GMI.

The three candidate meteorological data sets are described in section 2. To distinguish among them, aspects of transport thought to be important to the stratospheric assessment were identified, and tracer simulations to examine these transport issues were designed. These simulations are described in section 3. The tests themselves and the model performance on the tests are presented in section 4. Some discussion and conclusions, including the choice of the meteorological data to be used in the assessment, are given in section 5.

2. Meteorological Input Fields

2a GMI-CCM2

The GMI-CCM2 meteorological fields (hereafter referred to as CCM2) come from a middle atmosphere version of the community climate model version 2 (MACCM2). The standard configuration of the community climate model [*Hack et al.,* 1994] is modified to produce a simulation appropriate for the stratosphere by reducing the horizontal resolution and increasing the vertical resolution. The middle atmospheric model is run at a horizontal resolution of about 2.8° latitude by 5.6° longitude, with 44 levels in the vertical extending from the surface to about 75 km. Near the tropopause the spacing between levels is about 1 km; the maximum vertical spacing is about 2.5 km. This model configuration provides a tropospheric simulation that is similar to the standard version of the model and a realistic stratospheric simulation. The meteorological fields compare well with observations of winds and temperatures in the northern hemisphere [*Boville,* 1995]. However, the southern polar winter climatology is 30-40 degrees too cold, and the polar night jet is at least 50 meters/second too strong. These meteorological fields were used in an off-line full chemistry simulation, and comparisons of the resulting constituent fields with observations are discussed by *Rasch et al.* [1995].

The standard CCM2 gravity wave drag parameterization, which strongly influences the model middle atmosphere circulation, assumed a zero phase speed gravity wave source originating solely from flow over subgridscale orography [*Boville*, 1995]. This source of gravity waves was augmented to provide for a more general source of gravity waves with non-zero phase speed arising from a variety of sources (shear instabilities, frontal propagation and convection) by adding separate zonally uniform sources for northern hemisphere, southern hemisphere and equatorial gravity waves. As a result of this change, the errors associated with an excessively strong jet and cold temperatures in the southern hemisphere winter night are dramatically reduced. The resulting

meteorological fields have been used for studies of the dynamics and photochemistry of the southern hemisphere [e.g. *Brasseur et al.*, 1997]. However, in the northern hemisphere winter, the revised version compares less well with meteorological data in that the temperature is somewhat too warm, stratospheric sudden warmings are produced too frequently, and the final warming occurs too early in the model spring.

Datasets from both configurations of the model were provided to the AESA effort. The meteorological winds from the revised version of MACCM2 were judged to provide a better representation of the stratosphere than the first version, in spite of the known biases between model and observations for the northern hemisphere winter. The tests described below utilize the dataset with the revised gravity wave parameterization.

2b GMI-GISS

The Goddard Institute for Space Studies (GISS) meteorological fields used in GMI come from a middle atmosphere version of the GISS general circulation/climate model using model 2′ physics. The standard GISS climate model is configured on 4° latitude by 5° longitude grid with 9 layers [*Hansen et al.*, 1983; *Rind and Lerner,* 1996]. The middle atmosphere model used here has higher vertical resolution (31 layers), an upper boundary at 80 km, and a gravity wave drag parameterization that greatly improves the simulation of stratospheric temperatures and the strength of the jets [*Rind et al.,* 1998 and references therein). The vertical grid uses sigma coordinates from the surface to 150 hPa and fixed pressure levels above to a model lid of 0.002 hPa. The layer thickness is about 2 km near 150 hPa and increases to about 4 km throughout the stratosphere. The GMI-GISS (hereafter referred to as GISS) chemical transport simulations use the 6 hour averaged wind and temperature fields recorded from a single year of this model. The top 4 layers (above 72 km) are combined into a single layer. Analysis of the dynamical properties of these wind fields is given by *Rind et al.* [1998] and references therein, and the use of these wind fields in a CTM is described by *Hannegan et al.* [1998].

2c GMI-GEOS DAS

The GEOS DAS (Goddard Earth Observing System Data Assimilation System) winds are produced by a stratospheric version of the GEOS-1 system described by *Schubert et al.* [1993]. The stratospheric version has the top raised to $\sim$ 0.1 hPa with a total of 46 vertical levels. The horizontal resolution is 2° latitude by 2.5° longitude. The vertical winds are mapped to a 29 level grid using a scheme which minimizes errors due to noise in the assimilated wind field. This technique integrates horizontal divergence over a column and maps the horizontal winds onto new vertical levels, while conserving the mass flux [*S. J. Lin*, personal communication]. Near the tropopause the vertical spacing is about 1 km; the spacing is about 2.5 km through the middle and upper stratosphere. The output fields are available four times per day.

Unlike the other data sets used in this study, the GMI-GEOS DAS winds and temperatures (hereafter referred to as GEOS DAS) are based on observations; the period for the assimilation is October 1995 through September 1996. The observations include rawinsonde and satellite temperature retrievals as well as surface observations and cloud track winds. A short GCM forecast (3 hr) provides the first guess for an optimal interpolation data analysis procedure. The period used here is part of a longer assimilation run begun in May 1995 for the Stratospheric Tracers of Atmospheric Transport aircraft mission.

Some aspects of stratospheric data assimilation are described by *Coy and Swinbank* [1997] and *Coy et al.* [1994]. The global coverage from the satellite observations produces a good representation of the temperature and mass field. The mid and high latitude winds associated with the vorticity field are well represented through the use of the geostrophic approximation. In the lower stratosphere, additional information is provided by the middle latitude rawinsonde stations. At low latitudes the winds are less certain as there are not many rawinsondes which report tropical stratospheric data and the uniformity of the tropical mass field makes the geostrophic approximation

much less useful. The horizontal divergence of the wind field is not directly observed in the stratosphere. In the GEOS DAS products it is determined by the interaction of the general circulation model with the inserted observations. *Coy and Swinbank* [1997] showed that the GEOS DAS zonal mean divergence field produced a qualitatively correct residual mean meridional circulation; the tests described here evaluate the residual mean meridional circulation quantitatively.

3. Constituent Simulations

The primary goal of testing these wind fields is to evaluate their ability to produce realistic transport in the lower stratosphere. To this end, we performed several simulations of long-lived tracers, and tested the resulting fields against observations. All meteorological fields were used on a 4° latitude by 5° longitude horizontal grid; for some, this required interpolation. The number of vertical levels was maintained, unique to each model, as described in the previous section. Numerical transport was accomplished using a scheme developed by *Lin and Rood* [1996]. Only advective transport was considered. This is acceptable for the stratosphere, but for tropospheric simulations it will be necessary to include vertical transport by convection.

Nitrous oxide serves as a tracer of stratospheric transport. Its only sources are in the troposphere, and it is long lived in much of the stratosphere. Loss is prescribed from a photochemical model that used observed zonal mean climatologies for temperature and ozone. The loss frequency for N_2O (photolysis and reaction with $O(^1D)$) is tabulated as a zonal mean function of latitude, pressure, and month [*Hall and Prather*, 1995; *Avallone and Prather*, 1997]. Because N_2O is also the primary stratospheric source of reactive nitrogen NO_y, and because the observed correlation between NO_y and N_2O in the lower stratosphere is well defined and linear, the model NO_y behavior can be inferred from the model N_2O.

CO_2 serves as a tracer of upper tropospheric/lower stratospheric transport. Unlike

N_2O, it has no sinks in the stratosphere, but a small source from the oxidation of CH_4. Air enters the stratosphere at the tropical tropopause, where the CO_2 mixing ratio has both an annual cycle (3-4 ppmv) and an annual trend ($\sim$ 1.5 ppmv). Thus the phase of the CO_2 annual cycle in various regions of the lower stratosphere contains information about transport and mixing. The CO_2 simulations were forced at all model levels below 700 hPa with monthly zonal mean CO_2 mixing ratios derived from the NOAA Climate Monitoring and Diagnostic Laboratory (CMDL) global network of surface stations (*Pieter Tans*, personal communication). The CMDL data from remote stations were degraded to monthly values at 10° latitude bands. This 16-year record of CO_2 was used to force the CTM simulations by resetting the lower troposphere zonally every time step with the appropriate monthly value. This approach has been shown to produce reasonable simulations of CO_2 in the upper troposphere and stratosphere [*Hall and Prather,* 1993]. The small source of CO_2 from the oxidation of CH_4 could be calculated by simulating the stratospheric CH_4 distribution, but does not affect the propagation of the tropospheric signal in CO_2 into the lower stratosphere and is neglected here.

Including a convective parameterization in the tropospheric constituent transport was found to violate the separation of the upper troposphere and lowermost stratosphere for CCM2 and GEOS DAS (see test 5 below). Because stratospheric transport is of primary importance to the AESA assessment, the simulations considered here are run without convection; lack of convection is compensated for by applying the model lower boundary conditions up to the middle tropsophere. Because subsonic aircraft fly near the tropopause in the upper troposphere and lower stratosphere, it will be important that the GMI model used in SASS include a realistic and validated parameterization of convective transport.

4. The Tests

Figure 1 is a schematic representation of the stratosphere describing aspects of stratospheric transport which are important to model performance. The broad arrows on the diagram denote the Brewer Dobson circulation, which produces upward transport in the tropics and seasonally dependent downward transport in the middle and high latitudes. The thick solid line, with breaks in the subtropics, represents the tropopause, i.e., the level in the atmosphere at which the temperature, which generally decreases with altitude in the troposphere, begins to increase with altitude as a result of heating from absorption of ultraviolet light by O_3. The tropopause is also marked by distinct changes in the mixing ratio of various constituents, including H_2O, O_3, and NO_y. A thick solid line indicates the 380K potential temperature surface, which is approximately the lowest potential temperature surface which is fully in the stratosphere. Mixing can take place on constant potential temperature surfaces, but it is also inhibited by dynamical transport barriers. Shaded regions represent the subtropical boundaries and the boundaries between the middle latitudes and the winter polar vortex. As at the tropopause, constituent observations show distinct, seasonally dependent, horizontal gradients in these areas, suggesting separation of the air masses. Between these shaded regions, there is mixing on constant potential temperature surfaces.

The numerals on the figure indicate the part of the stratosphere to which a particular test is most relevant. The largest pollutant mixing ratios are expected at the flight level of the aircraft, marked by an airplane on the figure. Test 1 considers the temperature where the largest perturbation is expected. Test 2 has two parts which examine the balance between the residual circulation and horizontal mixing in the middle to upper stratosphere (Test 2a) and in the lower stratosphere (Test 2b). Test 3 concerns the separation between the tropics and middle latitudes. Test 4 focuses on the vertical transport in the tropics and the effects of entrainment of air from the middle latitudes. Test 5 looks at transport near the tropopause. Test 6 concerns exchange

between the middle latitudes and the tropics.

These tests are comprehensive but not exhaustive. Furthermore, in this first incarnation of the GMI model, we have chosen to include one "typical" year for each of the meteorological data sets. There is no effort to assess the role of the quasi-biennial oscillation or other phenomena contributing to longer time scale variability. The accuracy of the model response to supersonic aviation (i.e., the HSCT assessment) is not likely to be equally sensitive to the model ability to match observations for each of these tests. However, the model performance on each of these tests provides an overall evaluation of the model transport, with the possibility that differences between model and observations can be understood in terms of physical processes. The tests and model performance are discussed in detail below.

Test 1 Temperature

The projected supersonic aircraft are expected to fly near 50 hPa, mostly at northern middle latitudes [*Prather et al.,* 1992]. Although the temperature *per se* does not affect the dispersion and buildup of aircraft exhaust, the processes affecting the impact of aircraft exhaust are temperature dependent, through gas phase photochemical reactions and through heterogeneous reactions on the surfaces of aerosols and polar stratospheric clouds (PSCs). In addition to the temperature dependence of some of the reactions which take place on aerosols and PSC surfaces (e.g., $ClONO_2 + H_2O$), the formation threshold for PSCs is temperature dependent, and the threshold itself will increase if the aviation products enhance the natural background of H_2O and HNO_3. This test focuses on the model climate at 50 hPa for two latitude bands, 40°N-50°N and 60°N-70°N. An annual climatology is compiled using 18 years of data from the National Center for Environmental Prediction (NCEP), formerly the National Meteorological Center (NMC). The monthly mean for the NCEP temperature includes all data within the specified latitude band for all 18 years; the monthly mean for the models includes

1 year. The standard deviation for each month is calculated using daily temperature fields and their difference from this monthly mean. The annual cycles of the monthly mean and standard deviation of NCEP temperatures for the two latitude bands are compared with the annual cycle and standard deviation for temperatures from CCM2, GEOS DAS, and GISS in Figure 2. At 40°N-50°N, GEOS DAS temperatures fall within the standard deviation of the NCEP climatology, as expected since the same data used to produce GEOS DAS are one year of the NCEP data set. CCM2 temperatures are within the standard deviation of NCEP most of the year, falling outside only during late summer and fall. The GISS temperatures are warmer than the NCEP climatology for most of the year. The standard deviations of the model fields generally follow the standard deviation of NCEP, except during winter when CCM2 and GISS show less variance than observed and GEOS DAS shows slightly more for 1995 compared with the 18 year climatology.

At 60°N-70°N, both CCM2 and GISS mean temperatures are 3 to 4 degrees warmer than the NCEP climatology for most of the year. This is a known deficiency of the version of CCM2 used for this test, as discussed in section 2a. Both CCM2 and GISS exhibit much less winter variance than NCEP (or GEOS DAS).

The differences seen in this figure are scored quantitatively using the following standard:

$$\text{grade}_\theta = 1 - \frac{1}{12}\sum_{i=1}^{12} \frac{\mid T_{\theta,i}^{MODEL} - T_{\theta,i}^{NCEP} \mid}{2\sigma_{\theta,i}^{NCEP}} \qquad (1)$$

where T is the monthly mean temperature, σ is the standard deviation from the monthly mean, θ refers to the latitude band and the subscript i refers to each of the 12 months. Thus the grade is high when the model difference from NCEP, weighted by the standard deviation of the NCEP temperatures, is small. Although it may be important for strongly temperature dependent processes such as PSC formation that σ^{MODEL} is smaller than σ^{NCEP}, such processes cannot be realistic if there is a large difference from the mean temperature, and we have chosen not to score the comparison of the observed

and modeled standard deviations. The scores for the three models are summarized in Table 1.

Test 2 Residual Circulation and Mixing

The strong vertical stability in the stratosphere constrains the vertical velocities to be a small fraction of the horizontal velocities. Thus, while the horizontal winds in the lower stratosphere are on the order of 10 ms^{-1} the average vertical velocities are measured as fractions of a millimeter per second ($\sim$ 0.001 ms^{-1})[*Mote et al.*, 1998]. Since most trace gases in the stratosphere are vertically stratified, the vertical motions, though small, create horizontal gradients between regions of mean upward and downward motion. Concurrent horizontal motions tend to reduce these average horizontal gradients by mixing. Although at any given moment, large gradients may occur locally during mixing and wave breaking, for this evaluation we are concerned with monthly to seasonal time averages over 10° or greater latitudinal bands. For multi-year assessments the driving winds must realistically capture both the horizontal mixing and the slower vertical motions. In other words, since the CTM calculates vertical motion consistent with the horizontal wind divergence, the driving winds must capture both the divergence of the horizontal winds (for the slow upward motion) and the vorticity of the horizontal winds (for the horizontal mixing).

The above can be made more explicit by considering the residual mean meridional circulation and the Eliassen–Palm (EP) flux divergence associated with a given wind field [see *Andrews et al.*, 1987, p. 128]. An accurate representation of the EP flux divergence requires that the waves, seen mainly in the vorticity field, have realistic amplitudes and phase structures. The model waves must also dissipate by wave breaking or radiative damping at appropriate latitudes and heights. An accurate representation of the residual mean meridional circulation requires that the model or data assimilation system which generates the winds have an accurate radiative transfer scheme and a

plausible sub-grid scale wave drag, in addition to an accurate representation of the EP flux divergence from the resolved waves. Realistic wave forcing is necessary for the downward control principle to produce a useful residual mean meridional circulation [*McIntyre*, 1992].

One way to judge the transport characteristics associated with a wind field is to study the long lived tracer distribution produced by the wind field through advection and mixing. *Randel et al.* [1994], by evaluating the zonal mean tracer budget, show how the long lived tracers depend on the residual mean circulation and eddy transport. These tests are designed to see how well the circulations associated with different driving wind fields can simulate the characteristics of an observed long lived tracer.

Test 2(a) Mid to Upper Stratosphere

Nitrous oxide N_2O is emitted in the lower troposphere and destroyed in the stratosphere by photolysis and by reaction with excited atomic oxygen $O(^1D)$. The latter reaction is by far the smaller process through which N_2O is destroyed (about 10%), but is the dominant source of reactive nitrogen species in the stratosphere. The local chemical lifetime of N_2O decreases from hundreds of years at 100 hPa to several weeks in the upper stratosphere; the height and latitude dependence of the loss combined with the residual circulation and horizontal mixing produce the distribution seen in Figure 3. The N_2O pictured here was observed by the Cryogenic Limb Array Etalon Spectrometer (CLAES) on the Upper Atmosphere Research Satellite (UARS) [*Roche et al.*,1993; *Roche et al.*, 1996]. CLAES viewed from 34 degrees latitude in one hemisphere to 80 degrees latitude in the other hemisphere for periods of about one month during which the orbit precessed. The spacecraft was then yawed to keep the cold side away from the sun, and CLAES viewed the opposite hemisphere. The data shown in Figure 3 were taken from several days before and after yaw maneuvers, and thus provide near global coverage. Figure 3a shows data taken between Sept. 18 and

Sept. 24, 1992 and Figure 3b shows data taken between Jan. 6 and Jan. 13, 1993. Data are averaged in 10 degree latitude bands from 80°S to 80°N. These observations reveal seasonal differences in N_2O. For example, in the northern hemisphere, the N_2O contours at middle latitudes are flatter during January than in September, and the high latitude contours show evidence of winter descent.

The September and January zonal mean distributions for the three models are compared with CLAES observations in successive panels of Figure 4. Inspection of the figures shows that all three models produce distributions that have many features in common with the CLAES observations. The maximum N_2O at any pressure is found in the tropics, and the N_2O decreases with altitude at all latitudes. The winter contours are flatter at middle latitudes in January than during September; their flat character indicates efficient planetary wave mixing. The upwelling region varies among the models, and is narrowest for CCM2. There are also obvious differences among the models relative to each other and relative to CLAES data. These comparisons are quantified by requiring agreement of the model fields with several features in the CLAES data. The annual mean N_2O is calculated averaging all CLAES observations that fall within specified latitude and altitude (pressure) ranges. The vertical ranges are about 5 km, centered on 30, 10 and 2 hPa. Horizontal latitude bands are 10 degrees wide and centered on 45°N, 45°S, and the equator. For the annual cycle comparisons, all data within a month at the appropriate pressure and latitude band are averaged. Linear interpolation is used to fill observational gaps; at most one month is missing.

The model value must be within 20% of the CLAES value for a score of 1, and within 40% of CLAES for a score of 0.5. The following comparisons are made:

1. Annual mean at 3 levels for each latitude band (9 points of comparison)
2. The vertical gradients for each latitude band (6 points of comparison)
3. The horizontal gradients for each pressure (6 points of comparison)
4. The annual cycle in the tropics (36 points of comparison)

5. The annual cycle in the northern middle latitudes (36 points of comparison)

6. The annual cycle in the southern middle latitudes (36 points of comparison)

The scores on each component of the test are weighted to have a maximum of 1, and the overall score on this test is the average of the above six components. Results are given in Table 2.

A sense of these comparisons is gained by considering monthly average profiles for CLAES and for each model, shown in Figure 5 for the three latitude bands. Near the equator, GEOS DAS best represents the CLAES data in both magnitude and profile shape. However, for both northern and southern middle latitudes, GEOS DAS profiles exceed observations. Furthermore, the profile shape is not consistent with observations. Between 40°N and 50°N, the CCM2 and GISS profiles are nearly coincident with each other and with CLAES profiles. Between 40°S and 50°S, CCM2 and GISS profiles approximate the shape of the CLAES profiles, but the GISS profile is systematically high and CCM2 is systematically low. Given good comparisons for at least one latitude band for each of the meteorological fields, it is clear there is no simple conceptual model of changes in the residual circulation or horizontal mixing that will resolve the discrepancies. For example, stronger upwelling in the tropics would improve agreement of CCM2 and GISS with CLAES profiles, but such a change is likely to impact the good agreement at middle latitudes adversely. For all three models, the profile shapes are similar for the three latitude bands, whereas for CLAES the tropical profile shape is distinctly different from the midlatitude profile shape. This qualitative discussion is quantified by the scores given in Table 2. CCM2 has the highest score overall. The relatively low scores are a good reflection of the general overall agreement suggested by Figure 4 but the important quantitative differences shown in Figure 5.

Test 2(b) Lower Stratosphere

Strahan et al. [1998a] have developed a lower stratospheric climatology for N_2O that is based on 175 flights of the ATLAS instrument on the NASA ER-2 between August 1988 and September 1997 [*Podolske et al.*, 1993]. Figure 6 gives contour plots of this climatology in northern fall and winter. The data shown here reflect many of the same features found in the CLAES data (Figure 3) - N_2O is largest in the tropics, and decreases with increasing potential temperature. The data reveal seasonal dependence, for example, lower mixing ratios of N_2O are seen in middle latitudes during the winter than in the fall.

For this application, mean profiles are calculated for three latitude ranges (35°S-50°S, 10°S-10°N; 35°N-55°N) and each of the four seasons, excepting 35°S-50°S during austral summer as there are no data for this time and location. These latitude ranges are chosen to exclude the polar vortex. The vertical range of the observations is 360 - 530 K (about 150 - 50 hPa). The range 380 - 500 K has the most observations, so this comparison is limited to that range; observations are averaged in 20 K vertical bins.

Model mean profiles are calculated for the same seasons, latitude ranges, and potential temperatures as the ER-2 climatology. Because these comparisons are concerned with the transport above 380K, the results are scaled so that the model mixing ratio is equal to the observed mixing ratio at 380K (the tropical tropopause), the effective lower boundary for the stratosphere for this calculation. This eliminates biases caused by model differences in tropospheric transport.

The fall (September-October-November) profiles from the models are compared with the climatological profiles in Figure 7. In the tropics, the models values of N_2O are generally within the range of observations. The decrease with altitude is well represented. At northern middle latitudes, the model profiles agree well with observed profiles in the lowest part of the stratosphere, but diverge with increased potential temperature. At the highest potential temperature included in this comparison, the

model means are 270, 266, and 258 ppbv for GEOS DAS, CCM2 and GISS respectively. All are significantly greater than the observed 224 ppbv.

For each season, the N_2O at each of the six potential temperatures in the climatological profile is compared with model N_2O. If the difference between the model and the climatology is within the standard deviation of the model, the maximum score of 1 is given. A score of 0.5 is given if the difference is within the sum of the standard deviations of the model and the observations. No points are given for greater differences. The total score is scaled by the maximum possible score, so that the final value of this test is 1. For this test, CCM2 receives a score of 0.68, GEOS DAS receives a score of 0.63, and GISS receives a score of 0.43. As for Test 2a, although model N_2O fields exhibit many characeristics of the ER-2 climatology, the differences are important. The models uniformly fail to reproduce the seasonal changes in N_2O between 440 and 500 K. Furthermore, the modeled N_2O is always higher than observations for this potential temperature range at middle latitudes. The discrepancies suggest that there is not enough descent at middle latitudes relative to the horizontal mixing between the tropics and middle latitudes, and that the seasonal changes in the balance between the residual mean circulation and the horizontal mixing are poorly represented. N_2O and total reactive nitrogen NO_y exhibit a tight, linear anti-correlation in both observations and in most models (not evaluated here). Therefore, we anticipate that the systematic high bias in N_2O will be accompanied by a systematic low bias in NO_y.

Test 3 Tropical Midlatitude Distinctness of

Although the difference between the mean of all N_2O observations on a pressure level in the latitude band 40°N to 50°N and and that in the band 5°S to 5°N (section 2a) provides a gross measure of the balance between transport by the mean winds and horizontal mixing, it provides little information about the sharpness and location of this tracer gradient. The meteorological processes responsible for mixing in and near the

subtropics exhibit spatial and temporal variability, suggested by the differences between the Fall and Winter distributions shown in Figure 3a and 3b (for example, note the change in the latitude of the maximum vertical gradient near 10 hPa). The sharpness of the horizontal gradient, as seen in Figure 3(b) in the northern winter hemisphere, is produced by the combined influence of the residual circulation and the horizontal mixing driven by planetary wave transport. It contrasts with the more constant horizontal gradient seen in the northern fall hemisphere (Figure 3(a)). Transport from the extratropics to the tropics has been the subject of recent analyses of satellite and aircraft observations (see references under Test 4). Somewhat less attention has been paid to transport in the opposite direction, i.e., tropics to extratropics [*Waugh et al.*, 1996; *Boering et al.*, 1994]. There is outflow from the tropics at all levels associated with upward transport, and the tracer distribution at middle latitudes depends upon a balance between the mean horizontal and vertical transport as well as mixing across the subtropics.

One aspect of the large scale structure in an observed or modeled N_2O field can be characterized by considering the shape of a probability distribution function (PDF), that is, a histogram of the tracer field. The observations are weighted to account for non-uniform spatial sampling, and histograms for the model fields are computed by binning after interpolating the model values on a pressure surface to an equal area grid [*Sparling et al.*, 1998]. PDFs were made for CLAES N_2O observations, using all measurements between 10°S and 45°N at 3 UARS standard levels (31.6, 14.7 and 6.8 hPa) for summer (June, July, August 1992), fall (September, October, November 1992) and winter (January, February 1993). PDFs were made for each of the models, using the same latitude domain and the model pressure level closest to the UARS level. GEOS DAS pressures are the same as UARS pressures, GISS pressures are 23.7, 23.3 and 7.5 hPa, and CCM2 pressures are 31, 15.9, and 7.8 hPa. The northern spring distribution is strongly influenced by the breakup of the polar vortex which varies greatly from year

to year, and is omitted from this analysis. Also excluded is the fall 1992 distribution at 31.6 hPa, as the CLAES observations are uncertain due to the Mt. Pinatubo aerosols. A total of eight distributions are compared. Results for 14.7 hPa are shown in Figure 8. The CLAES distributions are bimodal, i.e., there are distinct tropical and midlatitude peaks in the mixing ratio distribution for each of the 3 seasons shown at 14.7 hPa, and for each season considered at the other two pressure levels as well. For each case, the model is given a score of 1 if the distribution reveals two distinct air masses (i.e., if the distribution is bimodal) and 0 otherwise. However, as Figure 8 shows, in the models the midlatitude mixing ratios often appear as a tail appended to the tropical peak, rather than the separate peaks seen by CLAES. Note that this test is based only on the structure of the distribution; the relative heights of the peaks, the magnitude of their separation, their seasonal behavior, and the altitude dependence of the distributions are graded in Test 2.

The combined score is normalized to a maximum of 1. The CCM2 N_2O distributions shows two peaks for all 8 cases, giving CCM2 a score of 1. GISS shows two peaks in 5 cases and receives a score of 0.62, and GEOS DAS shows distinct air masses in only three cases, receiving a score of 0.38.

Test 4 Propagation of annual cycle

One focus of model evaluation is transport in the lower tropical stratosphere. The rates of tropical entrainment of extratropical air and upwelling within the tropics determine the rate at which midlatitude lower stratosphere HSCT effluent can reach the ozone layer. The vertical propagation of an annual cycle in tracer mixing ratio, forced by variations at the tropopause, stringently tests model transport in this region. Examples of such tracers are CO_2 [*Boering et al.*, 1994; 1996] and $\hat{H}$=H_2O+2CH_4 [*Mote et al*, 1996; 1998; *Randel et al*, 1998]. The phase speed is not necessarily the same as the mean upwelling rate in the tropics [*Hall and Waugh*, 1997a; *Mote et al*, 1996], but

in this case the two speeds are approximately the same. The attenuation of the signal amplitude is related to tropical entrainment of extratropical air and vertically diffusive processes within the tropics [*Avallone and Prather*, 1996; *Minschwaner et al.*, 1996; *Volk et al.*, 1996; *Hall and Waugh*, 1997b; *Mote et al*, 1998]. Here, properties of the modeled cycles are compared with estimates from *in situ* CO_2 and $\hat{H}$ observations taken during the Observations of the Middle Stratosphere (OMS) balloon campaign, [*Boering et al.*, "Timescales for stratospheric transport inferred from in situ observations of CO_2 from aircraft and balloons," manuscript in preparation, 1998], and HALOE $\hat{H}$, as analyzed by *Mote et al.* [1998] and *Randel et al.* [1998]. Data used here were provided by P. Mote and K. Boering. A similar comparison, employing a large number of models in addition to GMI, is made by *Hall et al.* [1998].

Figure 9 shows tropical profiles for the GMI models of (a) the cycle amplitude profiles (natural log scale) and (b) the phase lag time. (These profiles were derived from the models' simulation of the age spectrum, as discussed by *Hall et al* [1998].) Also plotted are the estimates from HALOE $\hat{H}$ data (square symbols) and from *in situ* CO_2 and $\hat{H}$ data (triangle symbols). There is good agreement between in situ and satellite inferences of phase, and both show that the models propagate the annual cycle signal too rapidly, i.e., the modeled phase lags increase too slowly with height.

For the amplitude, the *in situ* inferences at the two highest altitudes are considereably less than the corresponding HALOE values. On the one hand, HALOE is known to underestimate the annual cycle in H_2O at the tropopause [e.g., *Mote et al*, 1996] implying a possible overestimate of the fractional amplitude aloft. On the other hand, these top two *in situ* values are derived from the fewest number of balloon flights and may not be representative. In any case, the GMI model amplitudes bracket the observations. However, when proper account is taken for bias due to too rapid phase propagation (see below), all the models are seen to overattenuate the annual cycle.

Figure 9 shows that to a first approximation, models and measurements display

simple exponential decay of amplitude (a straight line fit to the log amplitude) and uniform phase speed (a straight line fit to the phase lag). Thus, the cycle propagation grade has 2 components, measured by single numbers: first, the average phase speed c from 16 km to 24 km; and second, the amplitude attenuation factor R. R is defined as H_a/λ, where H_a is the scale height of the exponential amplitude fit, and λ is the wavelength of the cycle (the phase speed times one year). R isolates the effectiveness of processes that attenuate the cycle better than H_a. As a measure of attenuation per wavelength, R summarizes the attenuation that occurs in each model over the same amount of time, 1 year. On a per wavelength basis, all the GMI models over-attenuate the annual cycle.

Each model grade has three possible values: 1 if the model value falls within the uncertainty range from observations; 0.5 if the value is within 50% of either the upper or lower bound of the observational range; and 0 if the value is 50% greater than the upper bound or 50% less than the lower bound. Table 3 summarizes the model performance, the individual grades for phase and amplitude, and a mean of the 2 grades.

Test 5 Separation of the Upper Troposphere and Lower Stratosphere

This test concerns transport in the lowermost stratosphere, and the possibility of substantial vertical mixing between the lowermost stratosphere and upper troposphere. *Nakazawa et al.* [1991], using a 2 year data set collected from commercial aircraft, report a CO_2 seasonal cycle in the upper troposphere (UT) near 60°N with a May maximum. At about the same latitude in the lower stratosphere (LS), 10-12 km, the observed amplitude of the CO_2 annual cycle was smaller, with a September maximum. These observations indicate a strong barrier to upward motion at the high latitude tropopause, which is the basis for this test. The model tropopause is identified using model temperature fields. The tropopause is determined by the temperature minimum and/or a decrease in lapse rate to less than 2K/km. For GEOS DAS and CCM2, which both

have vertical resolution of about 1 km near the tropopause, the two model levels nearest the tropopause (identified using the above criteria) are considered the tropopause levels. For GISS, which has vertical resolution of about 3 km near the model tropopause, only one level is used. The model level just above the tropopause is considered 'purely stratospheric' while the level just below is considered 'purely tropospheric'. The zonal mean of the CO_2 time series for each model at 60°N is evaluated. The observations show a 4 month difference between the maximum observed in the UT and that observed in the LS. A model is given a score of 1 if this difference is at least two months. While a model lag of 2 months is obviously significantly different from the observed lag, such a time interval is long enough to show that the seasonal cycle in the model lower stratosphere arrived via the tropical tropopause and not by vertical transport directly from the middle latitude troposphere because the tropical to midlatitude lower stratospheric lag is less than 2 months [*Boering et al.*, 1994]. Thus satisfying this criteria is sufficient to claim that the pathway for model transport is realistic. All three models score 1 on this test when no convective transport is implemented. However, convective transport as implemented with the GEOS DAS winds and the CCM2 winds causes both models to fail this test, while the GISS winds including convection pass this test [*Hall and Prather*, 1993]. In the GISS GCM convection is used to drive the general circulation which provides self-consistency between the convection and the mean circulation. Unlike the HSCT assessment, the SASS evaluation will require a realistic representation of convection, and this test will provide a strong constraint to the models.

Test 6 Horizontal propagation of the CO_2 signal

This analysis examines horizontal transport in the lower stratosphere but above the level of the tropical tropopause along quasi-potential temperature mixing surfaces. There are two aspects to this test. The first considers the amplitude of the annual cycle in CO_2, and the second considers the phase. As discussed by *Boering et al.* [1996] and

Strahan et al. [1998b], the extratropical CO_2 seasonal cycle between 380-440 K appears to be transported there from the tropics. Above 440 K, no clear CO_2 seasonal cycle is observed in the northern hemisphere midlatitudes. To identify the cycle originating in the CO_2 at the tropical tropopause unambiguously, it is necessary to eliminate the component of the cycle due to the residual circulation (i.e., temperature changes in the lower stratosphere that cause seasonal variations in the relationship between CO_2 and potential temperature). This is accomplished by evaluating the CO_2 seasonal cycle on N_2O surfaces rather than potential temperature surfaces. Here, the tropics are defined as 10°S to 10°N and the northern midlatitudes as 35°N to 55°N.

The amplitude test has two components. First, the model midlatitude seasonal cycle amplitude at 460 K must be less than 20% of the tropical seasonal cycle amplitude just above the tropopause (380 K). Second, the model seasonal cycle at 420 K in the midlatitudes must be at least 20% of the tropical seasonal cycle at 380 K. The models receive a score of 0.5 for each criterion which is satisfied. The GEOS DAS winds receive a score of 0.5; the CCM2 winds receive a score of 1. The GISS winds do not have sufficient native vertical resolution to make a meaningful application of this CO_2 amplitude test or the CO_2 phase test discussed in the following paragraph. when run in the GMI CTM using the *Lin and Rood* [1996] numerical transport scheme. Applications using a transport scheme which conserves second order moments resolves such vertical structures [*Prather,* 1986].

The CO_2 phase test, which is focussed on the lower stratosphere at potential temperature greater than or equal to that at the tropical tropopause, considers the phase of the CO_2 seasonal cycle in the midlatitudes relative to its phase in the tropics. *Boering et al.* [1996] and *Strahan et al.* [1998b] find that the observed midlatitude seasonal maximum between approximately 380K and 460 K appears about 2 weeks after it appears in the tropics. This demonstrates that the primary pathway for transport from the midlatitude troposphere to the midlatitude lower stratosphere is through the

tropics, rather than directly through the midlatitude tropopause. A model with a midlatitude seasonal maximum that arrives before the tropical CO_2 maximum implies an unrealistic pathway of transport in the model. For example, if the cycle maximum in the midlatitude LS arrived a few weeks after the maximum in the underlying troposphere, but before the arrival of the maximum in the tropics at the same height, this would imply unrealistic model transport directly up through the midlatitude tropopause. This test again uses N_2O as the vertical coordinate for CO_2. The N_2O bins (i.e., altitude ranges) are chosen to create 3 ranges between 380-460 K in the tropics. Three points are possible, one for each N_2O (altitude) ranges examined. The maximum score of 1 requires that the midlatitude seasonal maximum arrives 0.5-2 months after the tropical seasonal maximum. The score is 0.5 if the maxima appear within the half month temporal resolution of the analysis, and 0 if the midlatitude maximum precedes the tropical maximum. Both CCM2 and GEOS DAS receive a score of 1 on this part of the test, which indicates that horizontal transport is the dominant transport pathway. The GMI GISS results could not be diagnosed for this test. Results for both the CO_2 amplitude and phase tests are summarized in Table 4.

5. Discussion and Conclusions

The overall scores for the three models are given in Table 5. The CCM2 meteorological fields consistently outscored the GEOS DAS and GISS fields, and were selected for the GMI assessment of the stratospheric HSCTs. Clearly the process of grading and selection has just begun, and further comparisons will be part of a continuing model evaluation. For example, *Rodriguez et al.* [1999] extend these tracer tests to the full chemistry integrations. They compare the acuracy of these meteorological fields using the same chemical model with observed climatologies of column ozone and ozone profiles, with HALOE observations of NO and NO_2, and with an NO_y climatology for the lower stratosphere based on ER-2 data.

Although CCM2 is currently the best choice based on these tests, the tests also identify specific limitations to an assessment using CCM2 (as well as the GEOS DAS and GISS) meteorological fields. For example, because northern hemisphere winter temperatures are warmer than observed, the simulations with CCM2 fields will not predict polar statospheric clouds, nor will they simulate any increase in PSC occurrence due to the build up of H_2O and HNO_3 from the HSCTs.

A more important discrepancy identified here is the overestimate of N_2O in the lower stratosphere by all three models. Given the ready ability of most CTMs to match the observed N_2O-NO_y relationship in the lower stratosphere, it suggests that the models will significantly underestimate absolute abundance of NO_y near 20 km, the peak expected HSCT perturbation to NO_y. The modeled ozone response to this increase in NO_y is itself dependent on the base level of NO_y; the ozone change per ppb increase in NO_y is less negative for lower background levels of NO_y [*Wennberg et al.*, 1994] as expected for these meteorological fields.

Nevertheless, the identification of these drawbacks and assignment of grades points out the benefit of this approach in evaluating and selecting models for an assessment. A model which scores as well as GEOS DAS on Test 1 would be expected to provide a more realistic representation of PSC occurrence and perturbation by HSCTs given an appropriate model for PSC formation and evaporation, [*e.g., Considine et al.*, 1999]. However, it is misleading with such a single test to assume that some of the more complex interactions of chemistry and transport in the polar stratosphere (e.g., the isolation of the PSC-processed polar vortex) would then be accurately simulated by the model. Similarly, a model with a higher score on Test 2 is likely to have a reasonable NO_y background in the lower stratosphere, but this does not necessarily mean that the buildup of HSCT NO_y would be more accurate. Provided we pick a set of grading criteria that give a balanced test of model performance in simulating atmospheric observations, the model with the highest score can be defended as the best choice for

the current assessment.

Lastly, the establishment of formal criteria provides an objective baseline for evaluating new or improved versions of these meteorological fields in terms of their simulation of chemical tracers. As the general circulation models or data assimilation systems are developed and provide more realistic representations of stratospheric meteorology, these grades are likely to improve. However, neither GCM's nor data assimilation systems can simply be tuned to provide a bettter fit to these observations, thereby improving their grades. Simultaneous improvement in model performance on all these tests is not obvious (or likely). For example, developing a better parameterization for gravity-wave drag will affect both the residual circulation and temperatures, and while the mean winds and temperature may better match observations, the aspects of tracer transport as tested here may not improve. A better representation of stratospheric meteorology, necessary to develop a credible assessment model for HSCTs, cannot be achieved by fitting transport parameters to a set of mean measurements. It is vital to establish grading criteria such as used in this exercise that represent the range of atmospheric phenomena controlling atmospheric chemistry.

Acknowledgments.

We thank Kristie Boering and Phil Mote for providing additional analysis of their data sets, Mark Schoeberl for providing artistic talent in preparing Figure 1, and the rest of the GMI team for providing critical comments and suggestions throughout this project. This work was supported by The High Speed Research Program of NASA's Atmospheric Effects of Aviation Project.

References

Albritton, D. L., et al., The atmospheric effects of stratospheric aircraft: Interim assessment report of the NASA high-speed research program, *NASA Reference Publication 1333*, 1993.

Andrews, D. G., J. R. Holton, and C. B. Leovy, Middle Atmosphere Dynamics, Academic Press, Orlando, 489 pages, 1987.

Avallone, L. M. and M. J. Prather, Photochemical evolution of ozone in the lower tropical stratosphere, *J. Geophys. Res., 101*, 1457-1461, 1996.

Avallone, L. M. and M. J. Prather, Tracer-tracer correlations: three-dimensional model simulations and comparisons to observations, *J. Geophys. Res., 102*, 19,233-29,246, 1997.

Boering, K. A., B. C. Daube Jr., S. C. Wofsy, M. Loewenstein, J. R. Podolske, E. R. Keim, Tracer-tracer relationships and lower stratospheric dynamics: CO_2 and N_2O correlations during SPADE, *Geophys. Res. Lett., 21* 2567-2570, 1994.

Boering, K. A., S. C. Wofsy, B. C. Daube, J. R.!Schneider, M. Loewenstein, J. R. Podolske, and T. J. Conway, Stratospheric mean ages and transport rates from observations of CO_2 and N_2O *Science, 274,* 1340-1343, 1996.

Boville, B. A., Middle atmosphere version of CCM2 (MACCM2): annual cycle and interannual variability, *J. Geophys. Res., 100,* 9017-9039, 1995.

Brasseur, G. P., X. X. Tie, P. J. Rasch, and F. Lefevre, A three dimensional simulation of the Antarctic ozone hole: Impact of anthropogenic chlorine on the lower stratosphere and upper troposphere. *J. Geophys. Res., 100*, 8909-8930, 1997.

Considine, D. B., A polar stratospheric cloud parameterization for the three dimensional model of the global modeling initiative and its response to stratospheric aircraft emissions submitted to *J. Geophys. Res.*, 1998.

Connell, P. S., D. E. Kinnison, J. F. Lamarque, R. Ramaroson, R .J. Salawitch, D. B. Considine, S. R. Kawa, J. M. Rodriguez, D. A. Rotman, G. P. Brasseur,

J. R. Tannahill, "The global modeling initiative assessment model: Stratospheric photochemistry mechanism and solver , submitted to *J. Geophys. Res.*, 1998.

Coy, L., R. B. Rood, and P. A. Newman, A comparison of winds from the STRATAN data assimilation system to balanced wind estimates, *J. Atmos. Sci., 51*, 2309–2315, 1994.

Coy, L., and R. Swinbank, Characteristics of stratospheric winds and temperatures produced by data assimilation, *J. Geophys. Res., 102*, 25763–25781, 1997.

Douglass, A. R., M. A. Carroll, W. B. DeMore, J. R. Holton, I. S. A. Isaksen, H. S. Johnston, and M. K. W. Ko, The atmospheric effects of stratospheric aircraft: a current consensus, *NASA Reference Publication 1251*, 1991.

Douglass, A. R., R. B. Rood, C. J. Weaver, M. C. Cerniglia, and K. F. Brueske, Implications of thre-dimensional tracer studies for two-dimensional assessments of the impact of supersonic aircraft on stratospheric ozone, *J. Geophys. Res.,98*,8949-8963, 1993.

Douglass, A. R., C. J. Weaver, R. B. Rood, and L. Coy, A three-dimensional simulation of the ozone annual cycle using winds from a data assimilation system, *J. Geophys. Res., 101,* 1463-1474, 1996.

Graedel, T. E., D. Cariolle, M. Geller, J. Kerrebrock, D. Lister, K. Mauersberger, S. Penkett, U. Schmidt, S. Schwartz, and S. Solomon, Atmospheric Effects of Stratospheric Aircraft: an evaluation of NASA's interim assessment, *Washington D.C.: National Academy Press*, 45 pp., 1994.

Hack, J. J., B. A. Boville, J. T. Kiehl, P. J. Rasch, and D. L. Williamson, Climate statistics from the Natl. Cent. for Atmos. Res. community climate model CCM2, *J. Geophys. Res., 99,* 20,785-20,813, 1994.

Hall, T. M., amd M. J. Prather, Simulations of the trend and annual cycle in stratospheric CO_2, *J. Geophys. Res., 98*, 10573-10581, 1993.

Hall, T. M., amd M. J. Prather, Seasonal evolutions of N_2O, O_3, and CO_2; Three-dimensional simulations of stratospheric correlations, *J. Geophys. Res., 100*, 16,699-16,720, 1995.

Hall, T. M. and D. W. Waugh, Timescales for the stratospheric circulation derived from tracers, *J. Geophys. Res., 102*, 8991-9001, 1997a.

Hall, T. M. and D. W. Waugh, Tracer transport in the tropical stratosphere due to vertical diffusion and horizontal mixing, *Geophys. Res. Lett., 24*, 1383-1386, 1997b.

Hall, T. M, D. W. Waugh, K. A. Boering, and R. A. Plumb, Evaluation of transport in stratospheric models, *J. Geophys. Res., submitted*, 1998.

Hannegan, B., S. Olsen, M. Prather, X. Zhu, D. Rind, and J. Lerner, The dry stratosphere: A limit on cometary water influx, *Geophys. Res. Lett., 25*, 1649-1652, 1998.

Hansen, J., G. Russell, D. Rind, P. Stone, A. Lacis, S. Lebedeff, R. Ruedy and L. Travis, Efficient 3-D global models for climate studies: models I and II, *Mon. Weather Rev., 111,* 609-662, 1983.

Kinnison, D. E., et al., The Global Modeling Initiative assessment model: Application to high speed civil transport perturbation, submitted to *J. Geophys. Res.,*, 1998.

Ko, M. K. W., and C. H. Jackman, Second Models and Measurements, *Nasa Reference Publication*, 1999.

Lin, S. J., and R. B. Rood, Multidimensional flux form semi-Lagrangian transport schemes, *Mon. Wea. Rev., 124*, 2046-2070, 1996.

McIntyre, M. E., Atmospheric dynamics: Some fundamentals, with observational implications, in *The Use of EOS for Studies of Atmospheric Physics*, edited by J. C. Gille and G. Visconti, pp. 313-386, North-Holland, New York, 1992.

Minschwaner, K., A. E. Dessler, J. W. Elkins, C. M. Volk, D. W. Fahey, M. Loewenstein, J. R. Podolske, A. E. Roche and K. R. Chan, Bulk properties of isentropic mixing into the tropics in the lower stratosphere, *J. Geophys. Res., 101,* 9433-9440, 1996.

Mote, P. W., K. H. Rosenlof, M. E. McIntyre, E. S. Carr., J. C. Gille, J. R. Holton, J. S. Kinnersley, H. C. Pumphrey, J. M. Russell III, and J. W. Waters, An atmospheric tape recorder: the imprint of tropical tropopause temperatures on stratospheric water vapor, *J. Geophys. Res., 101*, 3989-4006, 1996.

Mote, P. W., T. J. Dunkerson, M. E. McIntyre, E. A. Ray, P. H. Haynes, and J. M. Russell, Vertical velocity, vertical diffusion, and dilution by midlatitude air in the tropical lower stratosphere *J. Geophys. Res., 103*, 8651-8666, 1998

Nakazawa,T., K. Miyashita, S. Aaki, and M. Tanaka, Temporal and spatial variations in upper tropspheric and lower stratospheric carbon dioxide, *Tellus, 43B*, 106-117, 1991.

Podolske, J. R. and M. Loewenstein, Airborne tunable diode laser spectrometer for tracer gas measurement in the lower stratosphere, Appl. Opt., 32, 5324-5333, 1993.

Prather, M. J., Numerical advection by conservation of second-order moments, *J. Geophys. Res., 91*, 6671-6681, 1986.

Prather, M. J., H. L. Wesoky, R. C. Miake-Lye, A. R. Douglass, R. P. Turco, D. J. Wuebbles, M. K. W. Ko, and A. L. Schmeltekopf, The Atmospheric effects of stratospheric aircraft: a first program report, *NASA reference publication 1272*, 1992.

Prather, M. J., and E. E. Remsberg (editors), The atmospheric effects of stratospheric aircraft: report of the 1992 models and measurements workshop, *NASA reference publication 1292*, 1993.

Randel, W. J., B. A. Boville, J. C. Gille, P. L. Bailey, S. T. Massie, J. B. Kumer, J. L. Mergenthaler, and A. E. Roche, Simulation of stratospheric N_2Oin the NCAR CCM2: Comparison with CLAES data and global budget analyses, *J. Atmos. Sci., 51*, 2834-2845, 1994.

Randel, W. J., F. Wu, J. M. Russell, A. Roche, and J. W. Waters, Seasonal cycles and QBO variations in stratospheric CH_4 and H_2O observed in UARS HALOE data, *J. Atmos. Sci., 55*, 163-184, 1998.

Rasch, P. J., X. Tie, B. A. Boville, and D. L. Williamxon, A three-dimensional transport model for the middle atmosphere, *J. Geophys. Res., 99*, 999-1017, 1994.

Rasch, P. J., B. A. Boville, and G. P. Brasseur, A three-dimensional general circulation model with coupled chemistry for the middle atmosphere, *J. Geophys. Res., 100,* 9041-9071, 1995.

Rind, D., 1996.

Rind, D., D. Shindell, P. Lonergan, and N. K. Balachandran, Climate change and the middle atmosphere. Part III: The doubled CO_2 climate revisited, *J. Climate, 11*, 876-894, 1998.

Roche, A. E., J. B. Kumer, J. L. Mergenthaler, G. A. Ely, W. G. Uplinger, J. F. Potter, T. C. James, and L. W. Sterritt, The cryogenic limb array etalon spectrometer (CLAES) on UARS: Experiment description and performance, *J. Geophys. Res., 98*, 10,763-10,775, 1993.

Roche, A. E., et al., Validation of CH_4 and N_2O measurements by the cryogenic limb array etalon spectrometer instrument on the Upper Atmosphere Research Satellite, *J. Geophys. Res., 101*, 9679-9710, 1996.

Rodriguez, J. M., P. Connell, D. Rotman, D. Kinnison, R. Salawitch, J. Logan, C. Scott, S. Strahan, The Global Modeling Initiative Assessment Model: Testing of model results against observations of chemically-active species, *J. Geophys. Res.*, 1999.

Rotman, D. A., J. M. Rodriguez, M. J. Prather, R. B. Rood, S. J. Lin, R. J. Rasch, T. Hall, D. Proctor, D .W. Waugh, J. R. Tannahill, The Global Modeling Iniative Assessment model: Model integration and testing of the transport shell, *J. Geophys. Res.,* 1998.

Schubert, S. D., R. B. Rood, and J. Pfaendtner, An assimilated dataset for Earth science application, *Bull. Am. Meteorol. Soc., 74*, 2331-2342, 1993.

Sparling, L. C., Statistical perspectives on stratospheric transport, *J. Geophys. Res., submitted* 1998.

Stolarski, R. S., S. L. Baughcum, W. H. Brune, A. R. Douglass, D. W. Fahey, R. R. Friedl, S. C. Liu, R. A. Plumb, L. R¿ Poole, H. L. Wesoky, D. R. Worsnop, 1995 Scientific Assessment of the atmospheric effects of stratospheric aircraft, *NASA Reference Publication 1381*, 1995.

Strahan, S. E., M. Loewenstein and J. R. Podolske, Climatology and small-scale structure of lower stratospheric N2O based on in situ observations, in press, *J. Geophys. Res.,*, 1998a.

Strahan, S. E., A. R. Douglass, J. E. Nielsen, and K. A. Boering, The CO_2 seasonal cycle as a tracer of transport, *J. Geophys. Res., 103*, 13,729-13,741, 1998b.

Volk, C. M., et al, Quantifying transport between the tropical and mid-latitude lower stratosphere *Science, 272*, 1763–1768, 1996.

Waugh, D. W., Seasonal variation of isentropic transport out of the tropical stratosphere, *J. Geophys. Res., 101*, 4007–4023, 1996.

Weaver, C. J., A. R. Douglass, and R. B. Rood, Tracer transport for realistic aircraft emission scenarios calculated using a three-dimensional model, *J. Geophys. Res., 100*, 5203-5214, 1995.

Weaver, C. J., A. R. Douglass, and D. B. Considine, A 5-year simulation of supersonic aircraft emission transport using a three-dimensional model *J. Geophys. Res., 101*, 20,975-20,984, 1996.

Wennberg, P. O., et al., The removal of lower stratospheric O_3 by free radical catalysis: *in situ* measurements of OH, HO_2, NO, NO_2, ClO and BrO, *Science, 166*, 398-404, 1994.

Received _____

[1]NASA Goddard Space Flight Center Greenbelt MD.

[2]Department of Geoscience, University of California at Irvine.

[3]Goddard Institute for Space Studies New York NY.

[4]General Sciences Corporation, Laurel MD

[5]National Center for Atmospheric Research Boulder CO

[6]Joint Center for Environmental Technology, University of Maryland Baltimore County

[7]Rosenstiel School of Marine and Atmospheric Sciences University of Miami.

Figure 1. This schematic shows the principle features of stratospheric transport; the numerals indicate aspects of transport which are the primary focus of a particular test. Test 1: the temperature distribution near the flight corridors; Tests 2(a) and 2(b): the residual circulation and horizontal mixing; Test 3: separation of the tropics and middle latitudes; Test 4: large scale ascent and horizontal mixing into the tropics; Test 5: separation of the troposphere from the lowermost stratosphere; Test 6: horizontal mixing from the tropics to the middle latitudes. The tests are described in detail in the text.

Figure 2. The annual cycles of the monthly mean and standard deviation of NCEP temperatures for the two latitude bands are compared with the annual cycle and standard deviation for temperatures from CCM2, GEOS DAS, and GISS

Figure 3. (a) CLAES N_2O averaged in 10 degree latitude bins from Sept. 18 to Sept. 24, 1992; (b) same as (a) but for Jan. 6 to Jan. 13, 1993.

Figure 4. The September and January zonal mean distributions calculated using winds from GISS (a and b); for CCM2 (c and d); for GEOS DAS (e and f).

Figure 5. Mean N_2O profiles for each CLAES and for each model for each month are shown for (a) 40-50S; (b) 5S-5N; (c) 40-50N.

Figure 6. Contour plots of and N_2O climatology in fall and winter derived from ATLAS measurements from the ER-2 during fall (a) and winter (b).

Figure 7. The fall (September-October-November) profiles from the models are compared with the climatological profiles. Each row corresponds to a different model (top: GEOS DAS; middle: CCM2; Bottom: GISS) and each column to a different latitude range (left: SH Middle; middle: Tropics; right: NH Middle).

Figure 8. Seasonal equal-area histograms of CLAES v.7 N_2O at vertical level 14.7 mb for summer (JJA 1992), fall (SON 1992) and winter (JF 1993). The shaded histograms are the model results, at vertical levels closest to the observations as indicated on the figure. Each row corresponds to a different model (top: GISS; middle: GEOS DAS; bottom: CCM2), and each column to a different season (left: summer; middle: fall; right: winter).

Figure 9. Vertical profiles in the tropics: (a), natural logrithm of the amplitude of the annual cycle in tracer mixing ratio propagating upward from the tropical tropopause; and (b), the phase lag time of the cycle. The amplitude is normalized to unity and the phase lag defined as zero at 16 km. Model profiles are (solid line) GISS 2', (short dash) CCM2, and (long dash) GEOS DAS. The symbols represent inferences from observations: (square) deductions from 5 years of HALOE-observed H_2O+2CH_4 data of *Mote et al*, [1998] (courtesy Philip Mote); (up triangles) in situ CO_2 measurements from 6 aircraft and 2 balloon deployments from 1994 to 1997; and (down triangles) in situ H_2O+2CH_4 from the same two 1997 balloon deployments (Boering et al., Timescale for stratospheric transport inferred from in situ observations of CO_2 from aircraft and balloons, manuscript in preparation, 1998; in situ data provided courtesy Kristie Boering).

Model Transport Tests

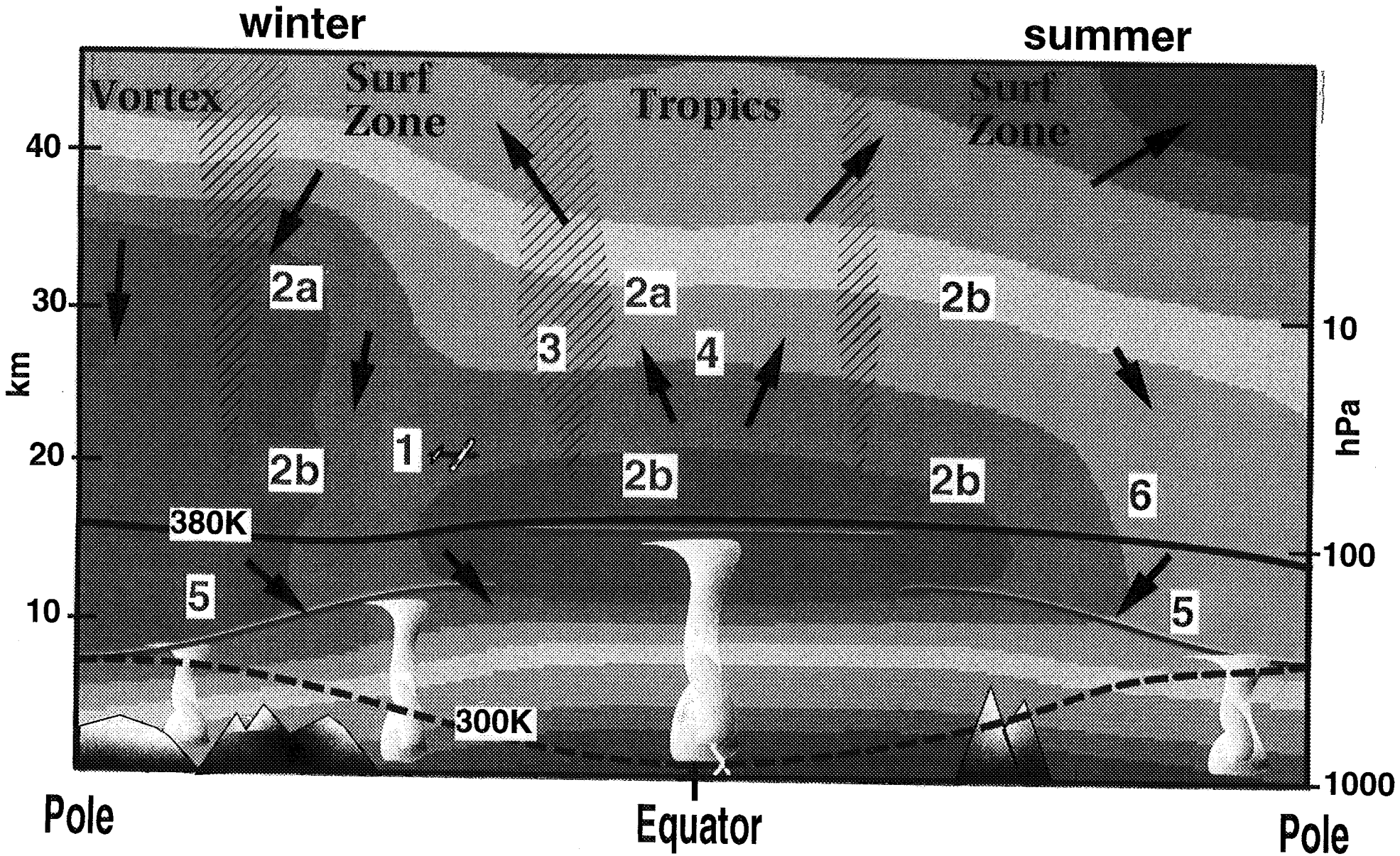

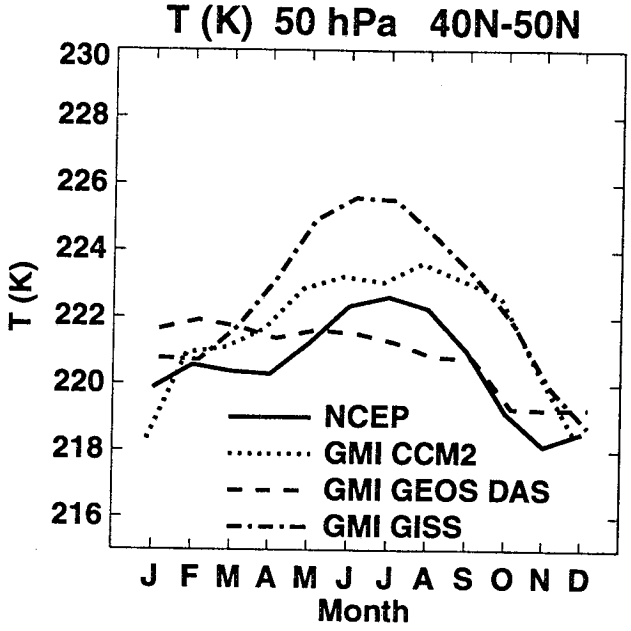
T (K) 50 hPa 40N-50N
T (K)
230
228
226
224
222
220
218
216
NCEP
GMI CCM2
GMI GEOS DAS
GMI GISS
J F M A M J J A S O N D
Month

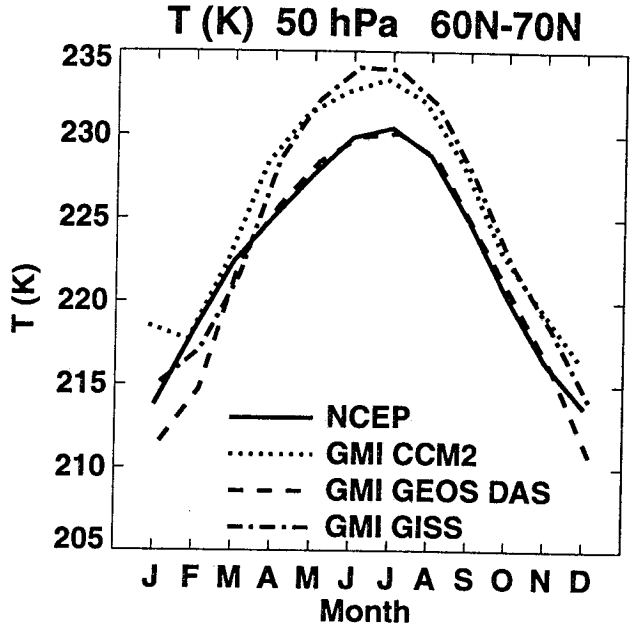
T (K) 50 hPa 60N-70N
T (K)
235
230
225
220
215
210
205
NCEP
GMI CCM2
GMI GEOS DAS
GMI GISS
J F M A M J J A S O N D
Month

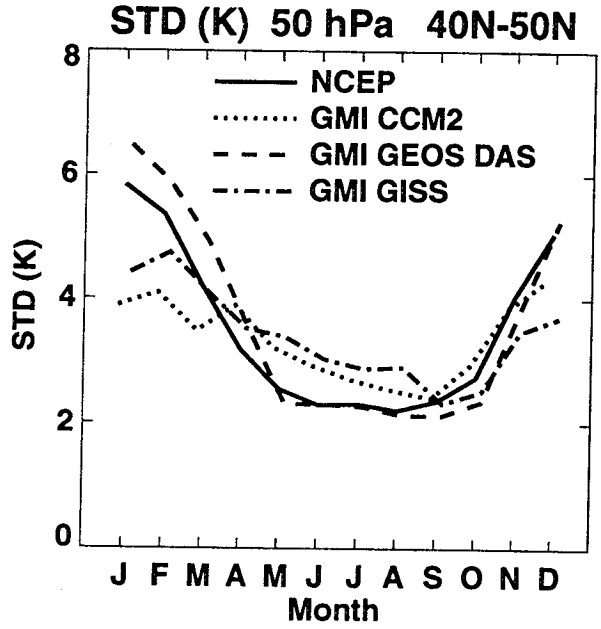
STD (K) 50 hPa 40N-50N
STD (K)
8
6
4
2
0
NCEP
GMI CCM2
GMI GEOS DAS
GMI GISS
J F M A M J J A S O N D
Month

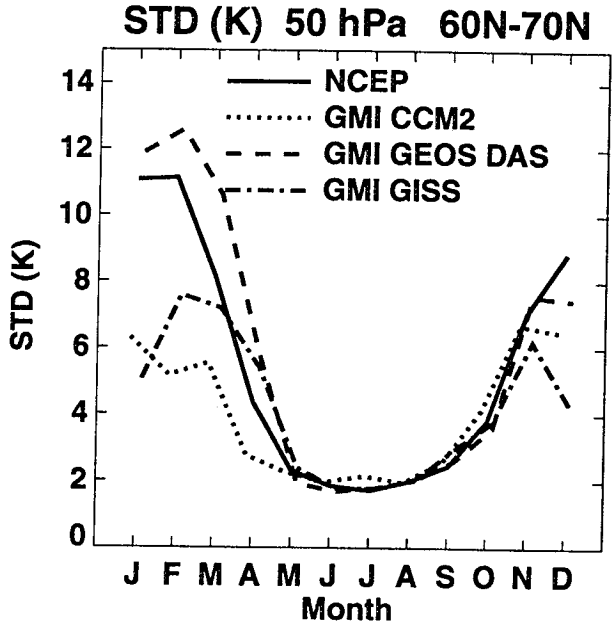
STD (K) 50 hPa 60N-70N
STD (K)
14
12
10
8
6
4
2
0
NCEP
GMI CCM2
GMI GEOS DAS
GMI GISS
J F M A M J J A S O N D
Month

FIGURE 2

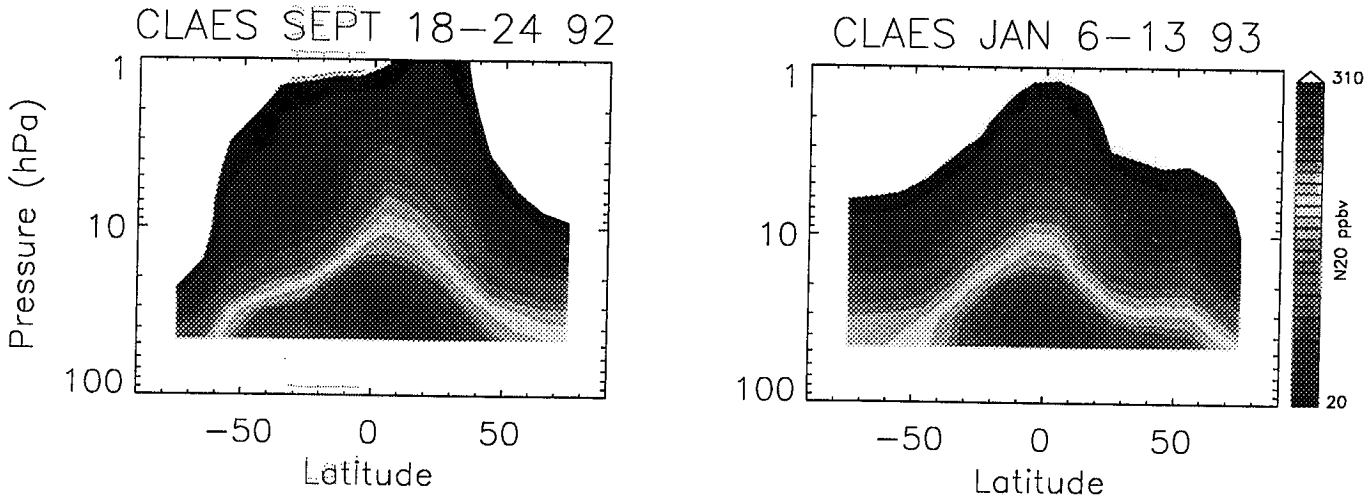
CLAES SEPT 18–24 92
CLAES JAN 6–13 93
Pressure (hPa)
1
10
100
−50
0
50
Latitude
310
20
N2O ppbv

FIGURE 3

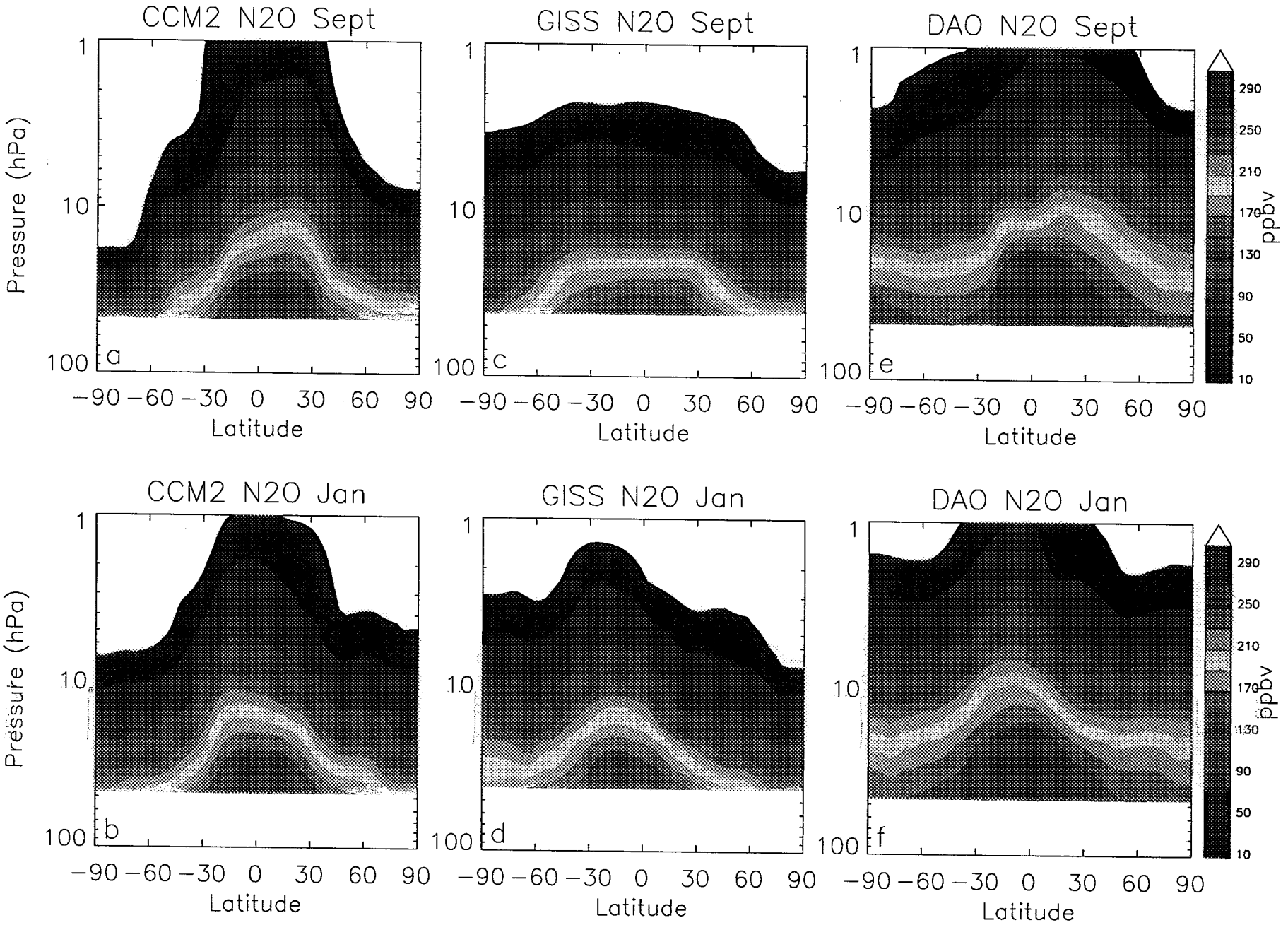
CCM2 N2O Sept
GISS N2O Sept
DAO N2O Sept
CCM2 N2O Jan
GISS N2O Jan
DAO N2O Jan
Pressure (hPa)
1
10
100
a
b
c
d
e
f
−90 −60 −30 0 30 60 90
Latitude
290
250
210
170
130
90
50
10
ppbv

FIGURE 4

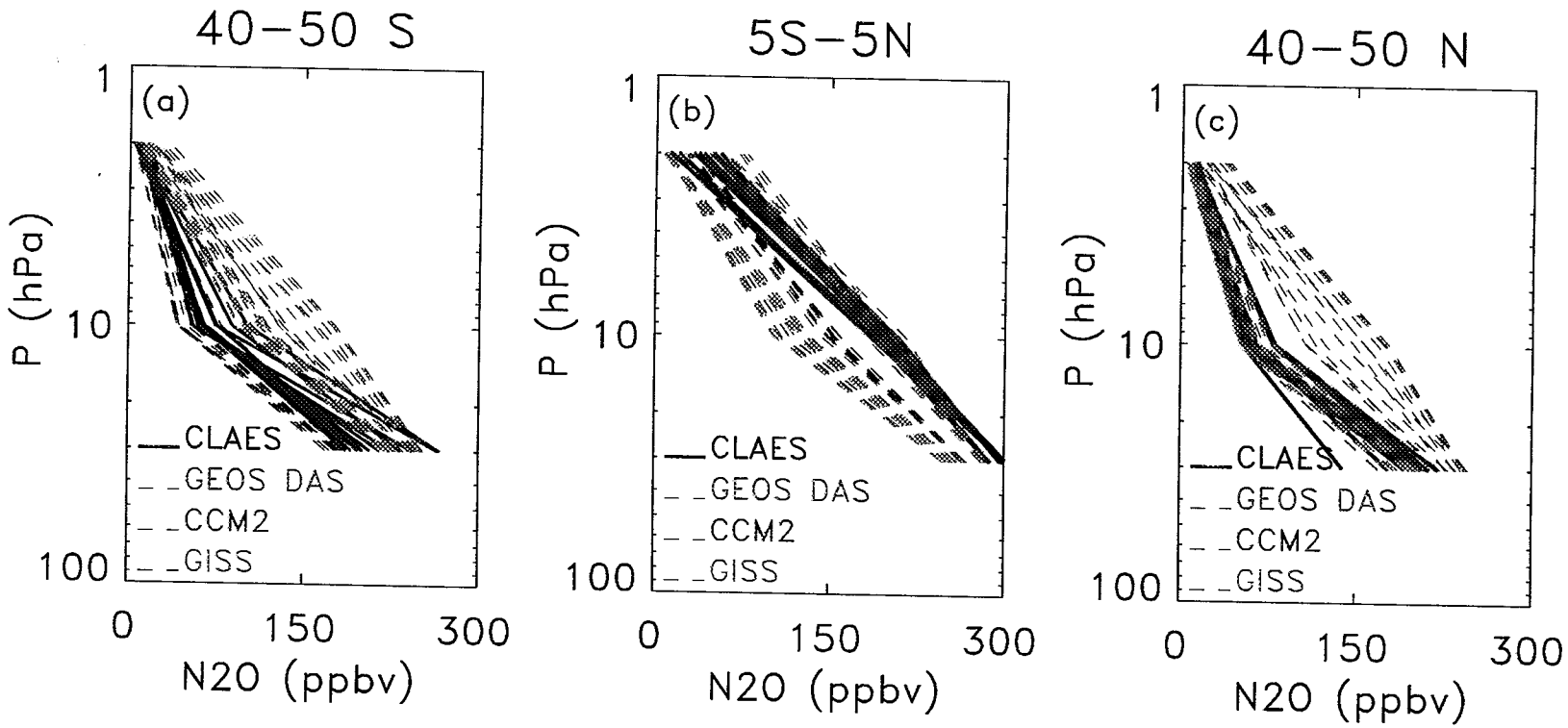
40–50 S
5S–5N
40–50 N
(a)
(b)
(c)
P (hPa)
1
10
100
0
150
300
N2O (ppbv)
CLAES
GEOS DAS
CCM2
GISS

FIGURE 5

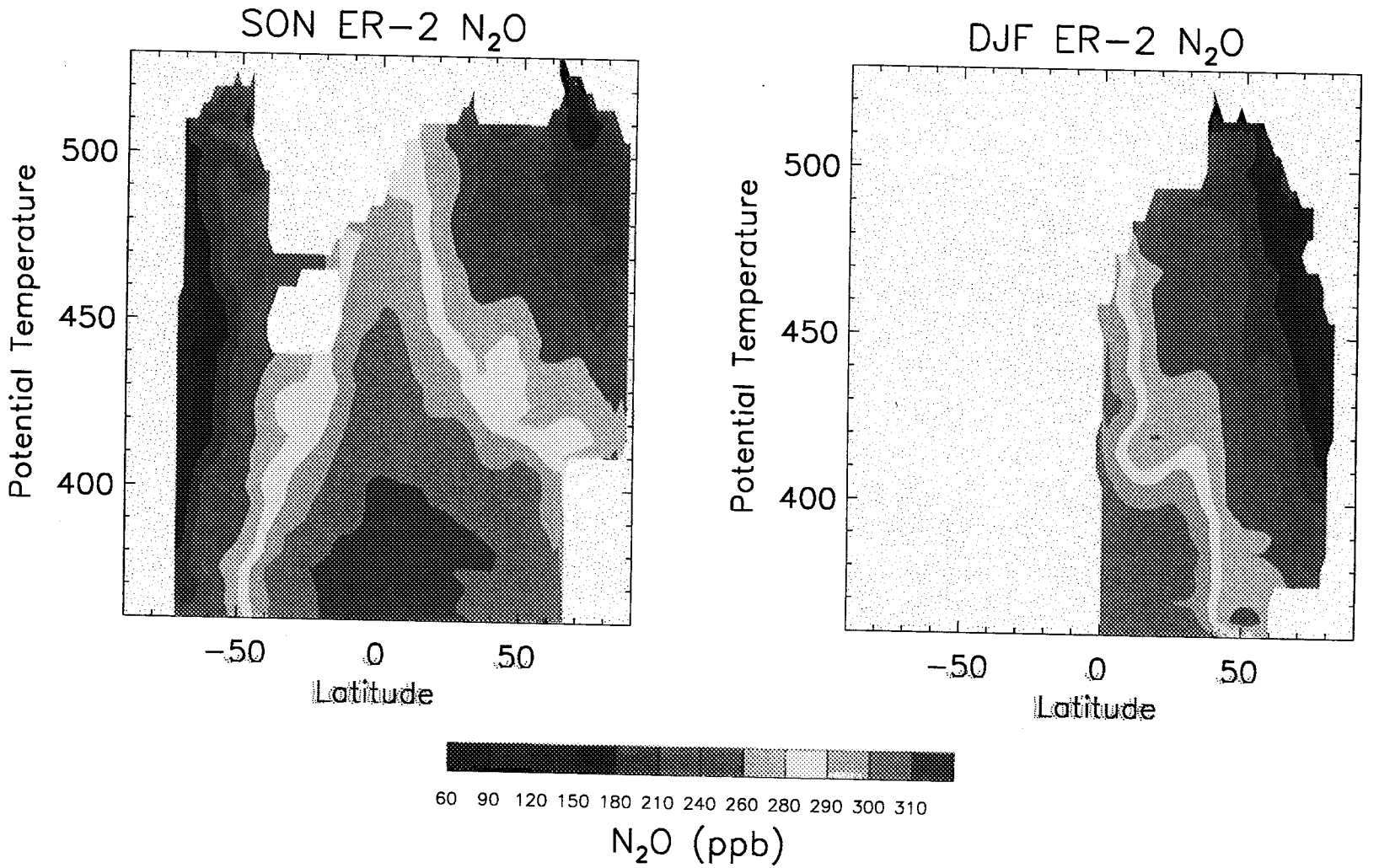
SON ER−2 N_2O
DJF ER−2 N_2O
Potential Temperature
500
450
400
−50
0
50
Latitude
60 90 120 150 180 210 240 260 280 290 300 310
N_2O (ppb)

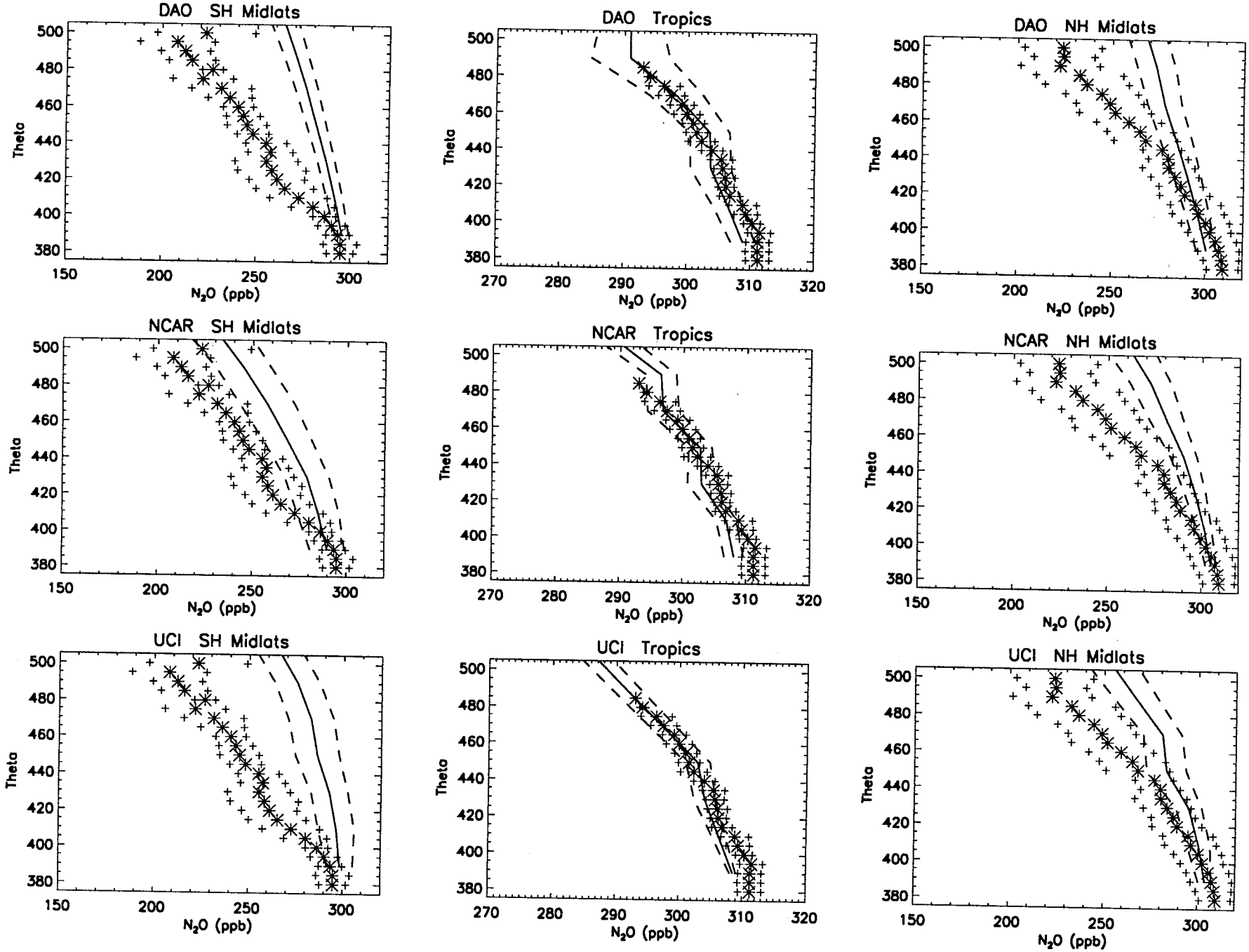
DAO SH Midlats
DAO Tropics
DAO NH Midlats
NCAR SH Midlats
NCAR Tropics
NCAR NH Midlats
UCI SH Midlats
UCI Tropics
UCI NH Midlats
Theta
N2O (ppb)

FIGURE 7

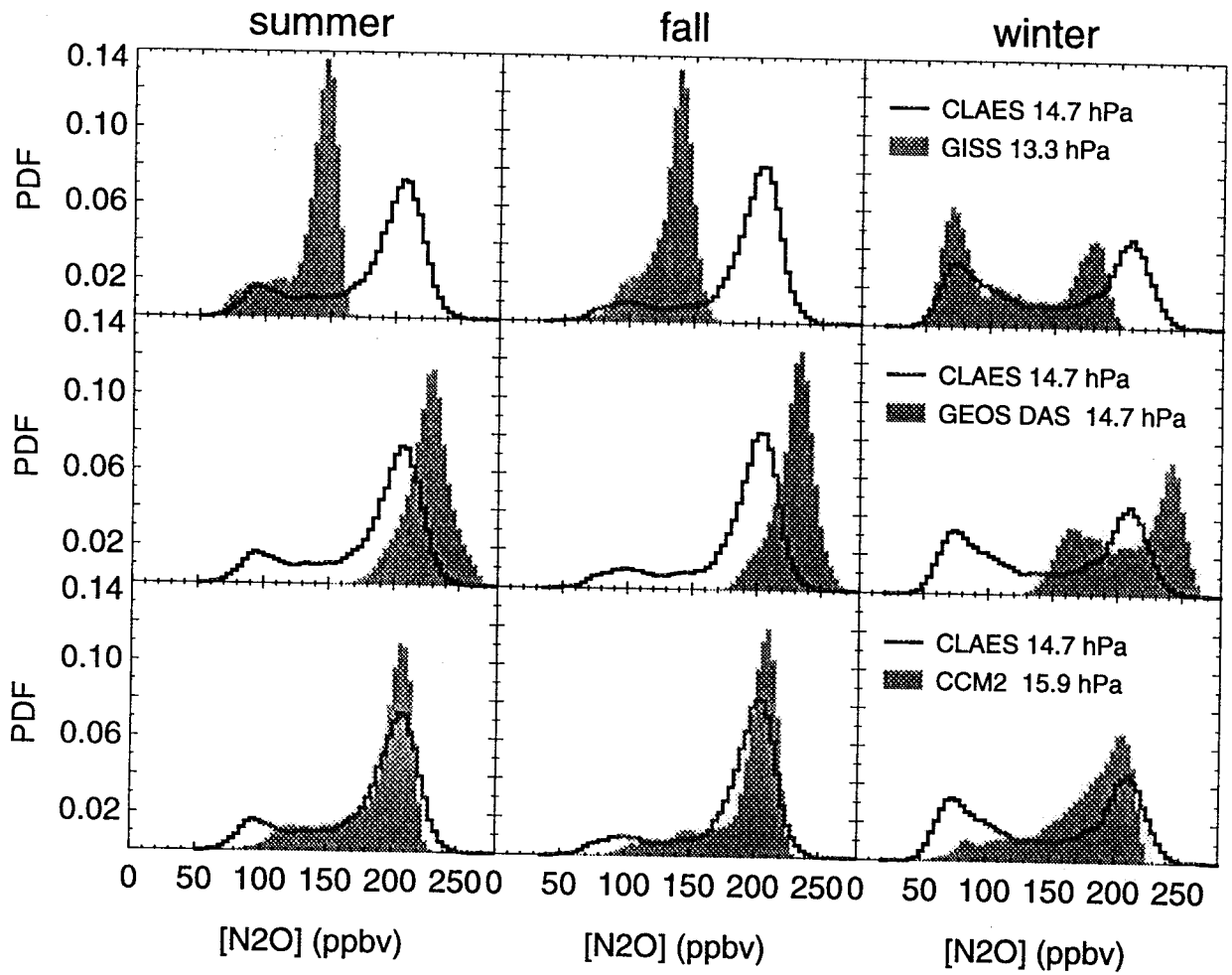
summer
fall
winter
PDF
0.14
0.10
0.06
0.02
CLAES 14.7 hPa
GISS 13.3 hPa
CLAES 14.7 hPa
GEOS DAS 14.7 hPa
CLAES 14.7 hPa
CCM2 15.9 hPa
0
50
100
150
200
250
[N2O] (ppbv)

FIGURE 8

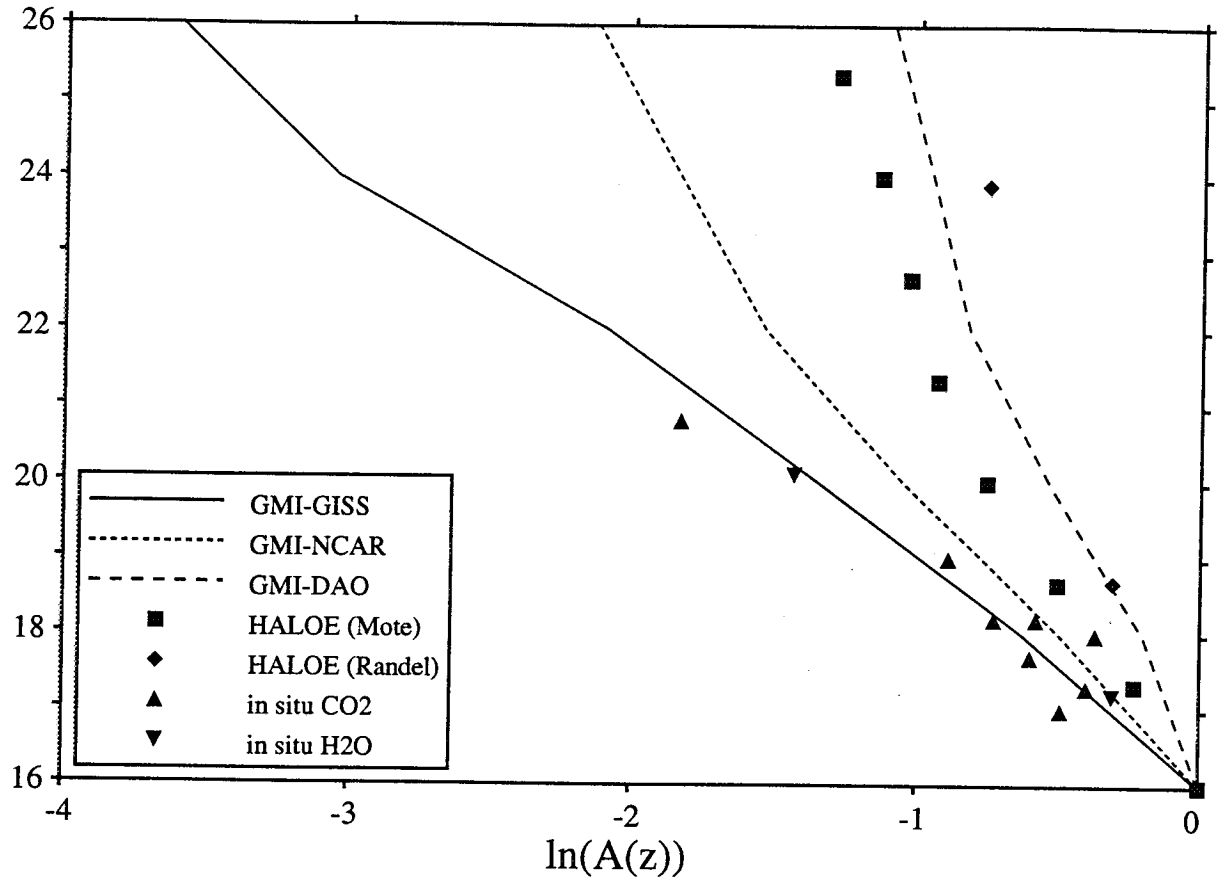
26
24
22
20
18
16
-4
-3
-2
-1
0
ln(A(z))
GMI-GISS
GMI-NCAR
GMI-DAO
HALOE (Mote)
HALOE (Randel)
in situ CO2
in situ H2O

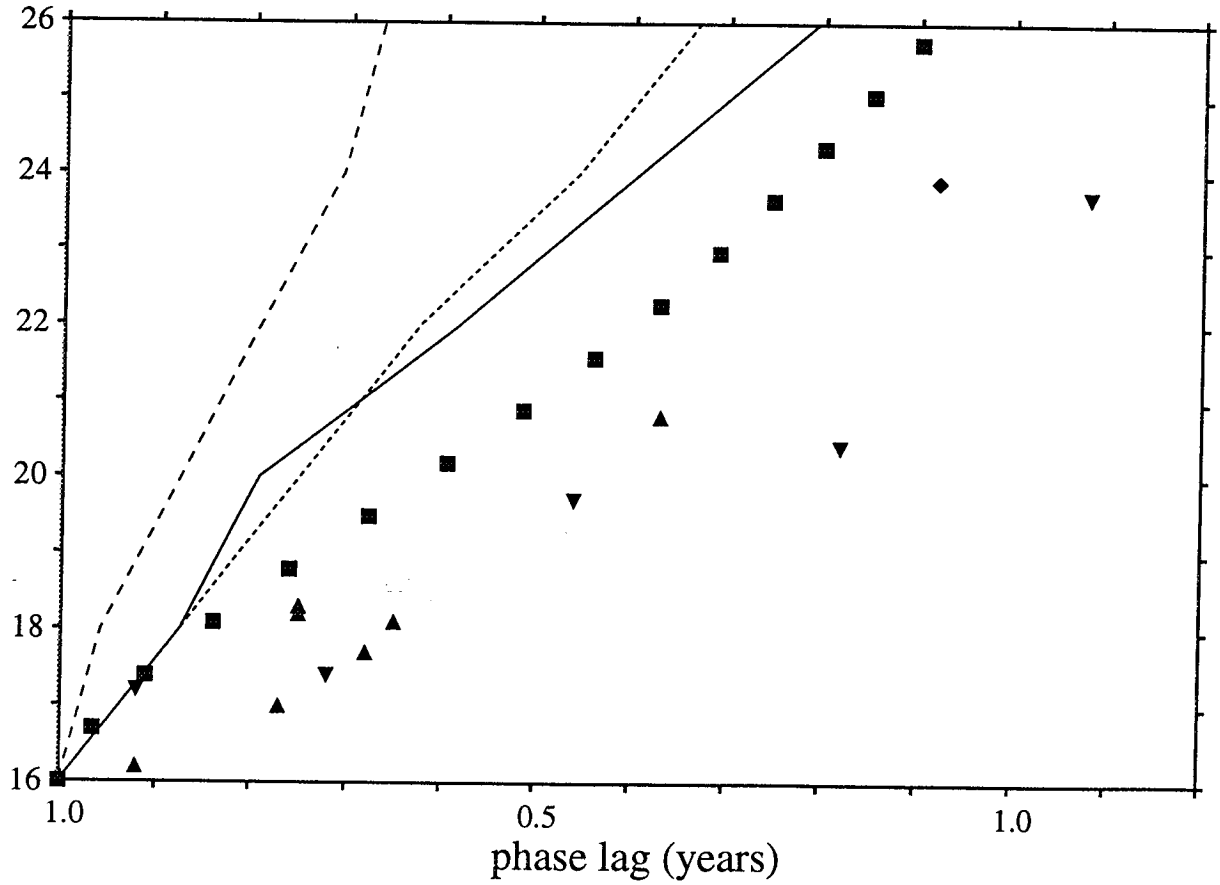
26
24
22
20
18
16
1.0
0.5
1.0
phase lag (years)